

**Tracking Study of 200 MeV Protons within a PMMA
Phantom**

By Nate Blumenkrantz

University of California, Santa Cruz

March 23, 2006

The thesis of Nate Blumenkrantz is approved by:

Professor Hartmut Sadrozinski
Thesis Advisor

Professor David Bellanger
Department Chair

Abstract

This paper describes an experiment that determined the position, and its associated uncertainty, of a proton at three different depths inside of a polymethyl-methacrylate (PMMA) absorber. These observed positions prove the fact that one can predict the most likely path (MLP) of a proton moving through a uniform medium, as long as the displacement and angle of that proton are known at the absorbers exit.

Introduction

Cancer patients with a malignant tumor near an important organ will most likely undergo conformal proton radiation therapy. Until a decade and a half ago, this type of radiation therapy was only available at physics laboratories that had particle accelerators. In 1990, the first clinical proton therapy center in the world opened at Loma Linda University Medical Center (LLUMC), in Loma Linda, California. Now there are two operating clinical proton therapy centers in the United States. The second opened in 2001 at the Northeastern Proton Therapy Center in Boston, Massachusetts [1].

When confronted with prostate or brain cancer, other methods of eradicating cancerous tissues are viewed as dangerous. X-ray radiation therapy, for instance, delivers an even amount of energy throughout the material that is contacted by the radiation beam. If an x-ray beam is pointed at a tumor in ones brain, the beam will not only damage and kill cells in the tumor, but will also damage and kill a great number of healthy brain cells.

The advantage of conformal proton radiation therapy is the fact that protons traversing a tissue lose the majority of their energy in a very short distance, directly before their trajectory terminates. Thus most of the protons energy can be deposited at a specific point rather than distributed evenly throughout a volume (like x-ray radiation). This results in the most accurate technique in eradicating cancer cells, while damaging the least amount of healthy tissue.

The weakness of this approach of cancer treatment, and the problem our group at the Santa Cruz Institute for Particle Physics (SCIPP), as well as our collaborators, are addressing, is the way proton beams are aimed at the patients tumor. Currently multiple x-ray images are obtained prior to the proton beam being activated, and then the patient is positioned in front of the proton beam according to the image of their tumor. Proton Computed Tomography (pCT) would make it possible to image with the actual proton beam. Therefore, one could position the patient with the beam at high energy that would be minimally harmful to the patient. And then, when the beam is properly aligned toward the tumor, the energy could be lowered to have the protons lose all their energy inside of the tumor, rather than after leaving the patient [2].

Computed Tomography (CT) is most popularly known for Computed Axial Tomography (CAT) scans. This is where a number of two-dimensional x-ray pictures are taken, and then used to create a three-dimensional image. Proton Computed Tomography would be similar, except instead of getting images by exposing the patient to x-rays (photons), a proton beam would be directed toward the patient, and the energy loss of each proton would be measured to identify the stopping power of the material the proton has traveled through. In order for this to work, a setup would need to be made which could measure the energy loss of the proton, and specific parameters, such as the exit displacement and angle, which could be used to determine the location of the proton when it traveled through the patient.

Energetic protons do not move straight through a medium, but instead, bend due to multiple coulomb scattering (MS) [3]. So when a proton is detected after traveling through a patient, its position inside of the patient cannot be determined exactly. Only the most likely path of that proton can be determined using the parameters mentioned in the above paragraph. Our collaborator, David C. Williams, wrote a theoretical paper predicting paths of protons given their exit displacements and angles [4]. The purpose of our experiment is to investigate the validity of this calculation.

Experimental Setup

Our apparatus was built around eight silicon strip detectors (SSDs). A single SSD can measure the position of a charged particle in one-dimension. To measure in three-dimensions, two detectors, plane 0 and plane 1, were glued extremely close together, forming what we refer to as a module. The strips on plane 1 were oriented in the vertical direction, and therefore measured the x-position, and the strips on plane 0 were oriented in the horizontal direction, measuring the y-position. Each of the four modules slid, one after the other in the z-direction, into one of ten slots inside our beam tracker box. This box was set in the path of a proton beam at LLUMC, with the modules and 12 pieces of PMMA arranged in three different positions. A total of six beam runs are analyzed, three runs each with different arrangements of modules and absorber plates, and three runs with the same setups except without the absorber present (see figure 1 for diagrams of the different runs). A calorimeter (an energy measuring device) was placed at the back of the box to measure the energy of each proton and trigger the data acquisition (DAQ) system [5]. In this analysis the energy loss was not analyzed.

The DAQ components start at the GTFE-32 chips that receive up to 32 channels, or silicon strips. The data are then serially read out into the fanout board, then through the field programmable gate array (FPGA), the translator board (which converted the signals to digital and sent them to the personal computer (PC)), and into the National Instruments DAQ card that interfaced the data streams with the PC's processor. The functionality of these components is described in more detail in reference [6].

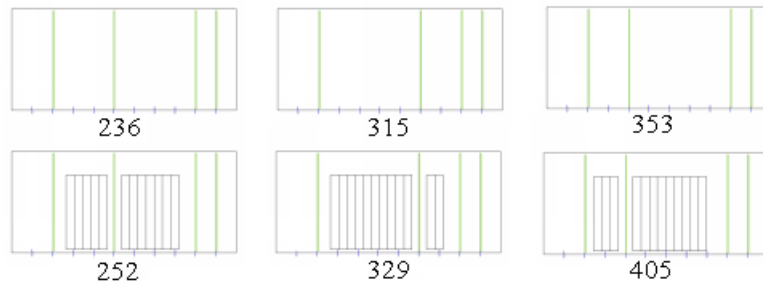


Figure 1: Six different detector and absorber set ups, one for each beam run. The beam is coming from left to right.

Procedure

To prove the prediction of a charged particles most likely path through a uniform medium, we had to measure the displacement of each proton at different depths inside of the PMMA. This was accomplished by placing one module in front of the absorber, a

second module (called the roving module) in between absorber plates, and the final two modules (called the rear telescope) behind the absorber (see figure 1).

Multiple beam runs were made, we look at six in particular, where the roving module is at three different depths, and for each roving depth, there is a run with absorber, and a run without absorber. When a beam run is performed, the calorimeter triggers on each proton, and assigns that proton a certain number that can be converted to energy. On each trigger, each silicon detector reports which specific channel (0 to 191) detected a proton. Sometimes multiple channels on the same detector report hits, or not every detector will detect the proton, these problem events will be discussed later in the paper. So ideally, each event will be associated with an energy, and record one hit on each detector.

This raw data, (event_id, module, plane, channel, and etc), is put into a file (called out.root) in the form of a T-Tree. These files are formed, and analyzed using ROOT, a data analysis framework for particle physicists.

Data Analysis and Results

I. Data cleaning and cuts

At first inspection of the raw data, by viewing channel histograms, one can easily see that there are hot channels (far too many hits), and dead channels (no hits), both of which could corrupt our analysis (see figure 2).

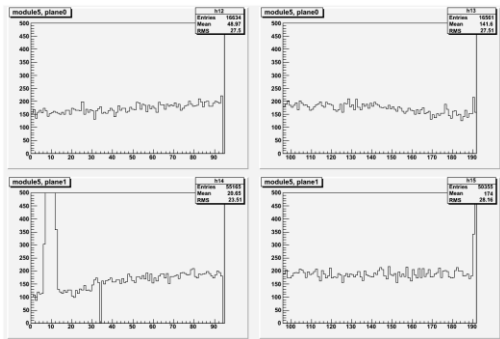


Figure 2: Channel histograms for plane 0 (top) and plane 1 (bottom), of the final module at the back of the telescope. One can see hot channels around channel 10 in plane 1, followed by a dead channel at about channel 34. This is raw data from an out.root file, from run 353.

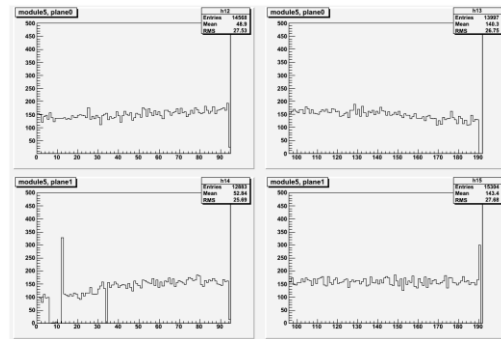


Figure 3: Channel histograms for the same planes as figure 2, but after clusterand reorder3.exe has cleaned the out.root file, and therefore masked the hot channels around channel 10, and got rid of multiple hits on the same plane by choosing the narrowest cluster.

The very first thing to do to our raw data is to mask out the hot channels. This task is performed using code written by J. Feldt (see clusterand reorder3.cpp in appendix B reference [7]). This code also deals with the fact that sometimes multiple channels on the same plane register hits during the same event. This happens if a chip malfunctions and relays that a certain channel was hit, and the channel that was actually hit reports a hit. Or if the proton was moving at such an angle that neighboring channels detected it at the same time. The way this was dealt with was to label multiple neighboring hits as clusters, and then, if there was more than one cluster in a plane for a certain event, pick the cluster with the smallest width as the actual hit for that plane and event. This results in a percentage of the events being misleading. The code should be altered to pick the

cluster that is closest to the hits on the corresponding planes on the module before, and the module after (in the z direction) the module in question. See figure 3 for a channel histogram after the discussed masking and clustering have been dealt with.

Next we run nate2.exe, which takes clusterandreorder3.root, creates a bunch of different arrays that make analysis easier, cuts all the events that have less than eight registered hits or more than 2 clusters, and produces nate2.root, which is the final ROOT file that we perform the rest of the analysis on. This final cut is important since data from all four modules is necessary to perform our analysis. It also produces some artifacts in the data. Since we masked out all of the hits around strip 10 on one module, most of the hits around strip 10 (and on plane 1) on the rest of the modules are cut since their event does not have planesHit=8 (but most likely has planesHit=7). This results in a depleted portion of the histogram around strip 10, plane 1, on every module. (See figures 4 and 5, there are other depleted portions of the histograms from other channels that were cut on a single plane.

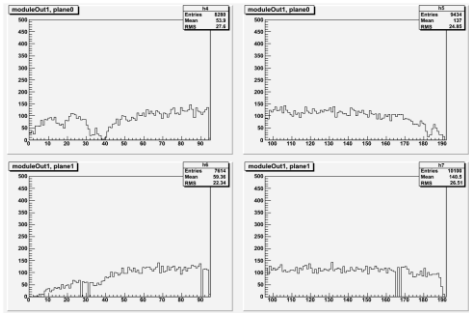


Figure 4: Channel histogram of roving module, showing how it was affected by the masked channels in the back module around channel 10, plane 1. These channel histograms are from a nate2.root file, for run 353.

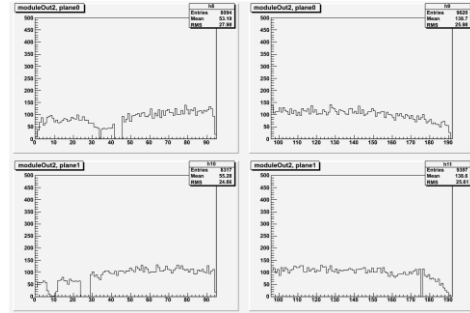


Figure 5: Channel histogram of the module in the front of the rear telescope, showing a depleted portion around channel 10, plane 1, due to the cut channels in the back module. These channel histograms are from a nate2.root file, run 353.

The following table shows how many events are lost for each specific run (with absorber) after each cut. When clustering and masking only entries are cut (hot channels and extra hits), resulting in practically zero events lost. But when we cut on the number of planes hit, we get rid of whole (useless) events, and in turn lose around $L = 45\%$ of data. This can be explained by the average efficiency (E) of about 90% per plane, $E^8 = 1 - L = 43\%$. The final column of table 1 will be discussed in the data analysis and results section of this paper.

Table 1: number of events in out.root, compared with number of events in clusterandreorder3.root, and nate2.root. The final column shows the number of events that are left after events with $-0.45\text{cm} < \text{materialExit} < 0.45\text{cm}$, and $-55\text{mrad} < \text{exitAng} < 55\text{mrad}$ are cut.

run:	raw events	clustered and masked events	planesHit=8 events	after parameter cuts
405	61,531	61,530	33,610	27,201
252	63,479	63,478	34,793	27,959
329	63,272	63,271	32,416	25,560

II. Detector alignment

We now have exactly eight hits per event, but we still need to align all the modules. If the modules were not pushed in all the way, or the detectors are attached to the modules at slightly different heights or depths, it can be hard to tell if a particles displacement is due to scattering or caused from misalignment of the detectors. This is fixed by setting the planes on the front module of the no absorber runs as the anchors, plotting the displacements of each entry on each subsequent plane, and then subtracting the mean displacement from each entry on each of the final 6 planes. The following plots (figures 6 and 7) show the average displacements on each of the planes, for each of the runs, absorber, and no absorber.

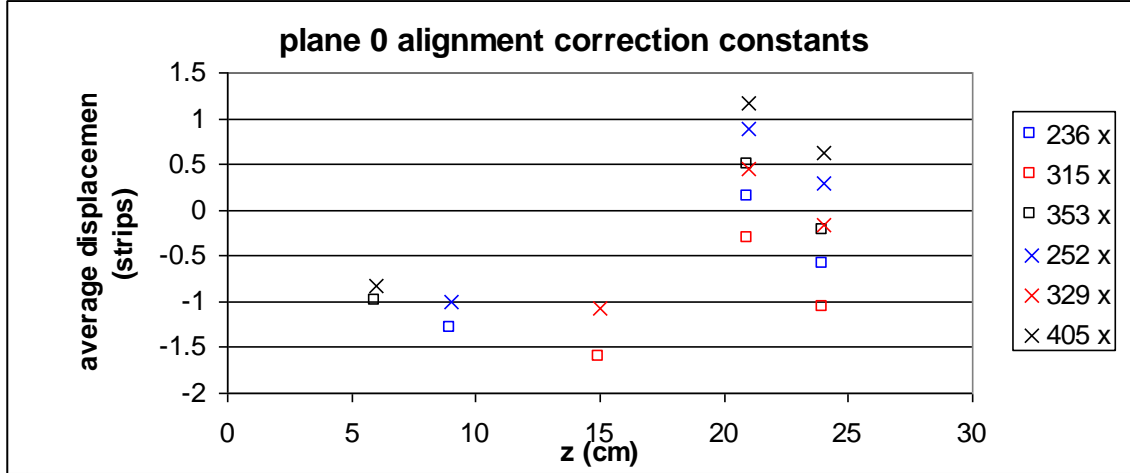


Figure 6: Average alignment corrections in the vertical plane for different runs. 1 strip equals 0.0236cm.

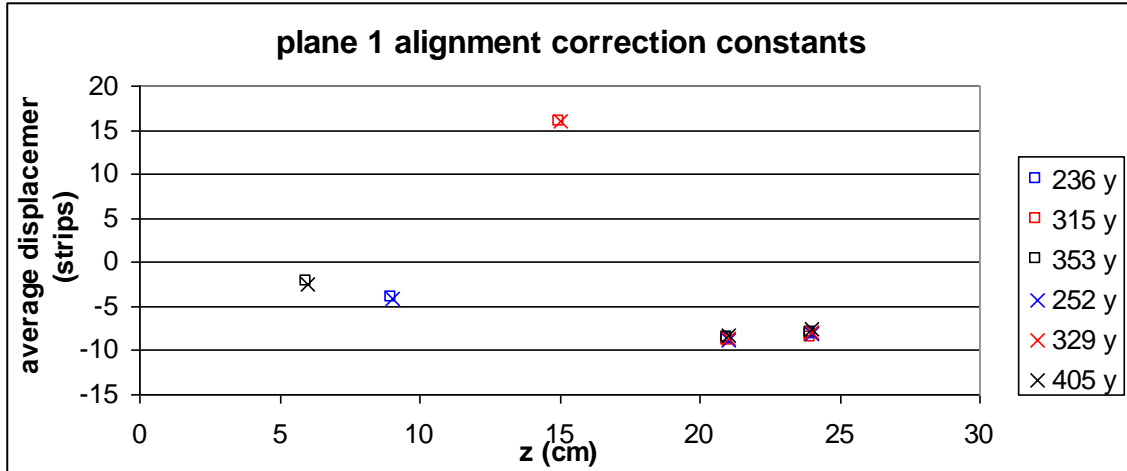


Figure 7: Average alignment corrections in the horizontal planes. Notice this plot is zoomed out much further than figure 6.

The conclusion we draw from this is that that plane 1 measures the x displacement, and there is more fluctuation in this direction since we are sliding the modules out of the box and into different slots. The numbers of the runs (236, 252, ...) indicate the times that the runs were performed.

III. Beam dispersion

As the proton beam progresses it spreads out. This is problematic since we are interested in the angle and displacement at the back of the absorber due to MS and not any other effects. To correct for these unwanted displacements and angles that are caused by this dispersion we plot two-dimensional correlation graphs of entrance position versus angle for no absorber runs. From these plots we obtain a linear fit which gives us the average angle of the trajectory depending on where the proton is at $z = 0\text{cm}$. This angle is then multiplied by the depth of each module to find the displacement caused by dispersion, which is then subtracted from the observed displacement, to obtain the actual displacement due to MS (see figures 8 and 9).

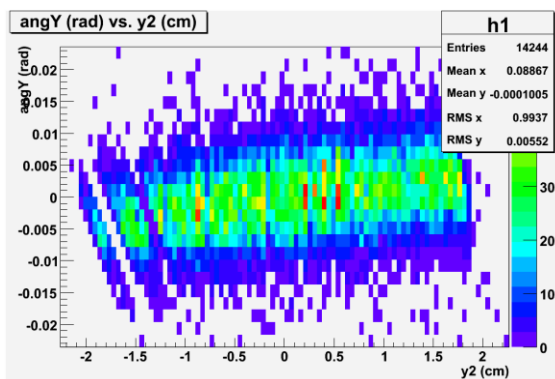


Figure 8: Correlation between entrance position and angle of protons, plotted in ROOT to see where most entries lie, for run 315.

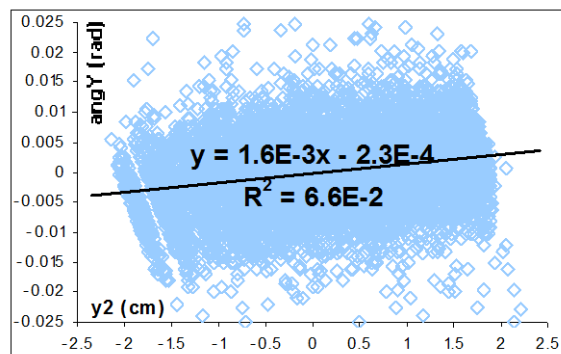


Figure 9: Correlation between entrance position and angle of proton, plotted in Excel to get linear fit which can be seen on graph (run 315).

After correcting for dispersion we again check alignment and notice there is a systematic offset during the absorber runs only (see figure 10). But since this offset is less than a strip, and within our final uncertainty, we do not follow up on this discrepancy. We do however subtract these average displacements from each entry on each corresponding plane and run.

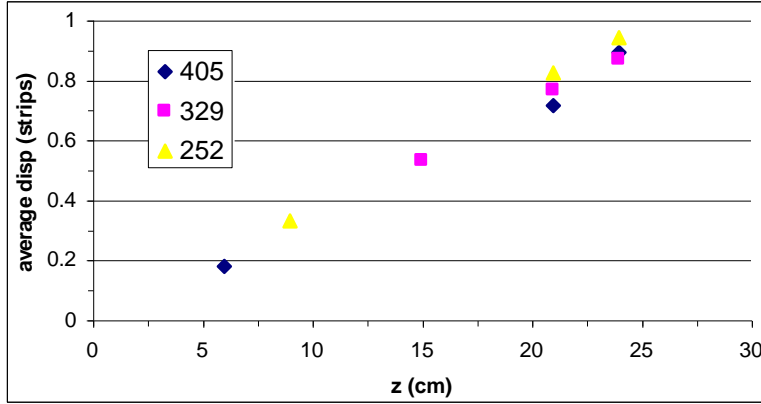


Figure 10: Plane 0 dispersion correction check, showing the average displacement on each plane for every absorber run after corrections for alignment and dispersion have been made. There still seems to be a small systematic offset.

IV. Experiment versus theory

The theoretical prediction of the displacement of the proton inside the phantom (on the roving module) is obtained by inputting two parameters: First, the displacement of the specific proton at the exit of the phantom called x_{mat} or y_{mat} , and, second, the change in the angle of that proton after traveling through the phantom, $exitAngX$ and $exitAngY$.

To fulfill the purpose of this paper we must compare the theoretical prediction with our experimental results for selected exit angles and displacements. And our first step is to determine what range of parameters makes sense to use (based on how many entries are dropped when cuts on the parameters are made, and what percentage of the leftover entries are bogus due to data cleaning errors). These cuts are determined, first, by plotting a two-dimensional histogram, of exit angle versus material exit displacement, and observing where the majority of the events lie (see figures 11, 12, and 13). Note that since our dispersion correction, discussed above, has rotated all particle trajectories to zero angle without the absorber present, all angles we detect on absorber runs are due to MS.

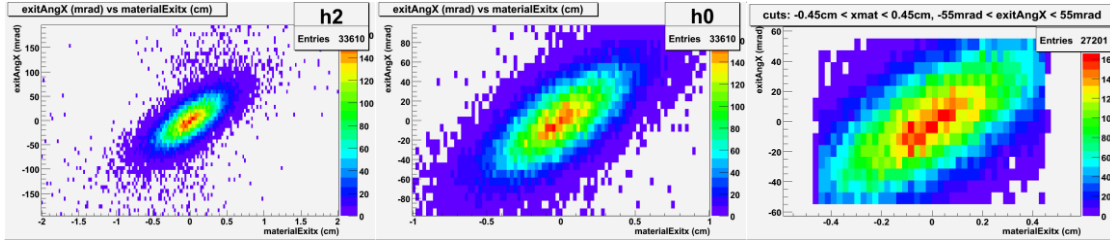


Figure 11: The angle the proton is leaving the phantom (exitAng) versus the displacement of the proton at the back of the phantom (materialExit or xmat) for plane 0, run 405.

Figure 12: Figure 11 slightly zoomed in. Note number of events in upper right of plot.

Figure 13: Shows how many events are lost for run 405 after cuts are made on all events with x mats outside of $\pm 0.45\text{cm}$ and exitAngs outside of $\pm 55\text{mrad}$. See new number of entries in upper right.

These plots show how few entries are lost when we make reasonable cuts on the parameters. In all cases no more than 20% of our data is lost. This assures that only events within limited range of displacement and angle are used, which would be well described by the gaussian approximations in the MLP calculation [4].

We decided to compare roving displacements for 9 different materialExits, and 5 different exitAngs: materialExit ($\pm 0.0200\text{cm}$) = -0.4, -0.3, -0.2, -0.1, 0, 0.1, 0.2, 0.3, 0.4, and exitAng ($\pm 5\text{mrad}$) = -50, -30, 0, 30, 50. Some combinations, materailExit = -0.4cm and exitAng = 50mrad for instance, did not make sense and were left out (too few entries), (see table 2 for which combinations were used). The bin sizes, ($\pm 5\text{mrad}$ and $\pm 0.02\text{cm}$), were chosen to correspond to the finite quantization of the SSDs (one strip every 236 μm).

For a sanity check, and to observe the dependence of the roving displacement on each parameter, we obtained our experimental results three different ways. We are indebted to our Italian collaborator Professor Mara Bruzzi, for suggesting two of the ways, which are discussed below.

First we fixed the exitAng to its five different values (± 50 , ± 30 , and 0mrad), plus or minus 5mrad, and, respectively, made five different plots of roving displacement vs. materialExit. We fit linear correlations to each plot, and therefore produced equations that made it possible to obtain roving displacement values for a continuous number of materialExit values, at fixed exit angles (see figures 14 and 15 for the 405 run xrov versus xmat correlation for protons with exit angle = $0 \pm 5\text{mrad}$). The plots for the rest of the exit angles can be found in appendix A.

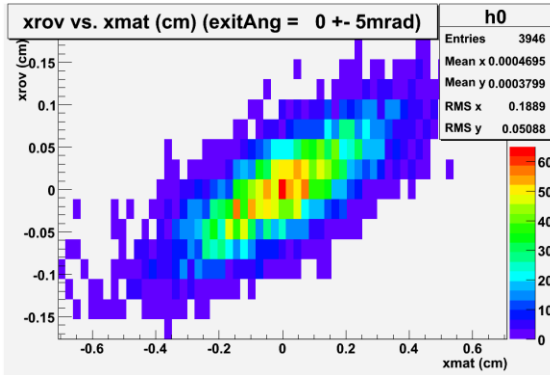


Figure 14: Roving displacement versus material exit displacement using ROOT, for all protons in run 405 with $-5\text{mrad} < \text{exitAngX} < 5\text{mrad}$.

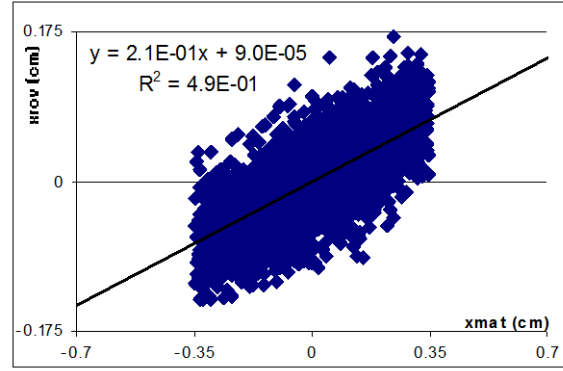


Figure 15: Same cuts on exitAngX as figure 14, as well as $-0.35\text{cm} < \text{xmat} < 0.35\text{cm}$.

With the linearly fit equations from the excel correlation plots we produce table 2, the run 405 horizontal and vertical displacements in the roving module. Tables 10 and 11 show similar results for runs 252 and 329 in appendix B. All materialExit values are $\pm 0.02\text{cm}$, and all exitAng values are $\pm 5\text{mrad}$.

Table 2: Roving displacement (cm) versus materialExit displacement ($\pm 0.02\text{cm}$) for different exit angles ($\pm 5\text{mrad}$) for run 405. The plane 1 (horizontal) displacements are on the right side.

ang	-0.4	-0.3	-0.2	-0.1	0	0.1	0.2	0.3	0.4	-0.4	-0.3	-0.2	-0.1	0	0.1	0.2	0.3	0.4
-50	-0.043	-0.025	-0.007	0.011						-0.047	-0.026	-0.004	0.017					
-30	-0.06	-0.04	-0.02	3E-04	0.02	0.041				-0.061	-0.041	-0.021	-0.001	0.019	0.039			
0		-0.062	-0.041	-0.021	9E-05	0.021	0.041	0.062			-0.06	-0.04	-0.02	6E-04	0.021	0.041	0.062	
30				-0.037	-0.018	0.001	0.02	0.04	0.059				-0.041	-0.021	-0.001	0.019	0.039	0.06
50						-0.014	0.006	0.026	0.046					-0.012	0.007	0.026	0.045	

The second technique is very similar to the first. The only difference is that we look at roving displacement vs. exitAng correlations with fixed materialExit displacements (see figures 16 and 17 for the run 405, materialExitx = $0 \pm 0.02\text{cm}$ xrov versus exitAngX correlation). The plots for the additional values of the material exit can be found in appendix A.

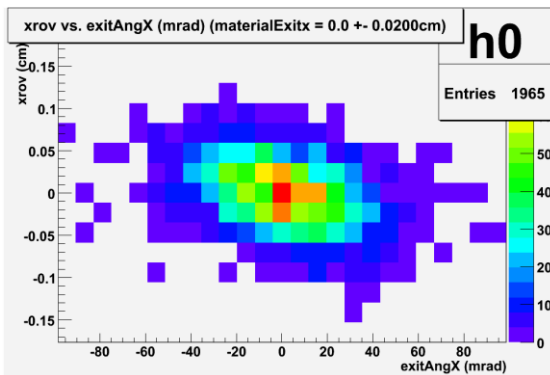


Figure 16: Roving displacement versus exit angle for fixed materialExit using ROOT, for all protons in run 405 with $-0.02\text{cm} < \text{xmat} < 0.02\text{cm}$.

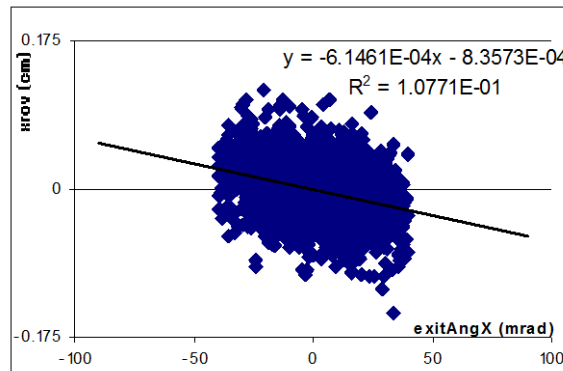


Figure 17: Same cuts as in figure 15 as well as $-40\text{mrad} < \text{exitAngX} < 40\text{mrad}$.

With these linear fits we produce table 3 below, for run 252, and tables 12, and 13 in appendix B, for runs 405 and 329.

Table 3: Roving displacement (cm) versus exitAng (+- 5mrad) for different materialExit displacements (+- 0.02cm) for run 252. The plane 1 (horizontal) displacements are on the right side.

ang	-0.4	-0.3	-0.2	-0.1	0	0.1	0.2	0.3	0.4	-0.4	-0.3	-0.2	-0.1	0	0.1	0.2	0.3	0.4
-50	-0.094	-0.061	-0.027	0.008						-0.097	-0.061	-0.024	0.012					
-30	-0.114	-0.079	-0.044	-0.01	0.027	0.06				-0.114	-0.08	-0.043	-0.006	0.028	0.065			
0		-0.107	-0.071	-0.035	0.002	0.035	0.071	0.107			-0.109	-0.071	-0.033	6E-04	0.036	0.07	0.106	
30				-0.061	-0.023	0.009	0.044	0.081	0.116				-0.061	-0.027	0.007	0.045	0.079	0.115
50						-0.008	0.026	0.063	0.098					-0.012	0.028	0.061	0.095	

In each of the first two correlation techniques, cuts were made on correlation parameters (i.e. on materialExit in figure 15 and on exitAng in figure 17). These cuts were made to improve the accuracy of our results, compared with the theoretical prediction. The accuracy is improved, with proper cuts, by eliminating the events that were affected by clustering errors (picking the wrong cluster), and also the events that are less likely (such as events with positive material exit displacement and negative exit angle and vice versa). It was found that if one made more stringent cuts it could improve certain results by 60um.

The third and final method we used to obtain experimental results was to simply plot one-dimensional histograms of the roving displacement for events within the selected range of materialExit displacement and exit angle (see figure 18, and figures A16 – A23 in appendix A). The means of these plots can be found in table 4 below and tables 14, and 15 in appendix B.

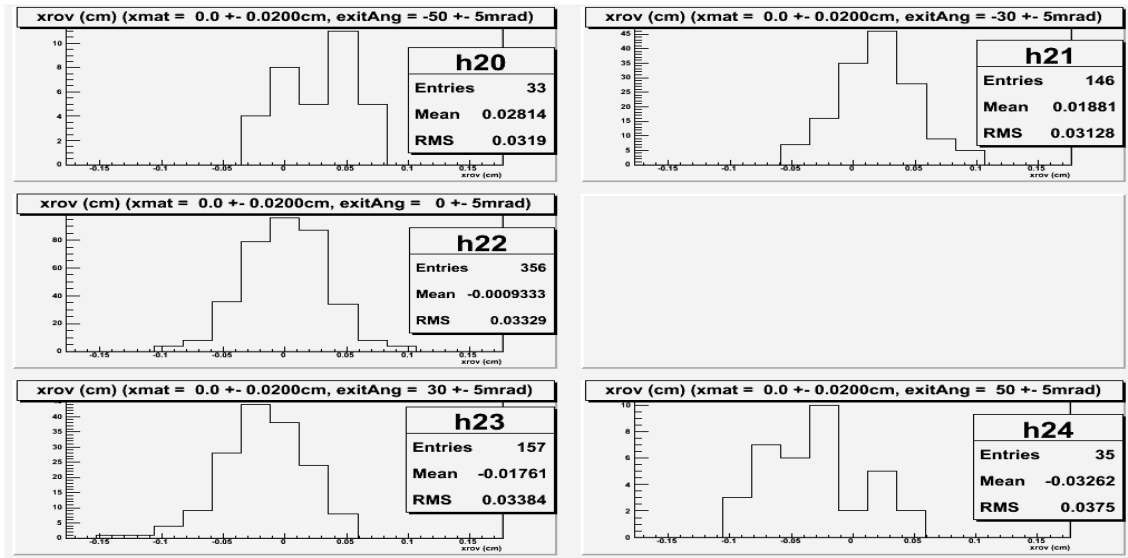


Figure 18: One-dimensional histograms of the roving displacement for protons with different materialExits and exit angles (cuts shown on titles of each histogram). The RMS in the legend on each histogram shows the spread (uncertainty) of the distribution. The number of entries, also in the legend, displays how many protons are within the specific cuts.

Table 4: Roving displacements for different combinations of fixed materialExit (+-0.02cm) and exitAng (+-5mrad) for run 329. The plane 1 (horizontal) displacements are on the right side.

ang	-0.4	-0.3	-0.2	-0.1	0	0.1	0.2	0.3	0.4	-0.4	-0.3	-0.2	-0.1	0	0.1	0.2	0.3	0.4
-50	-0.247	-0.179	-0.098	-0.035						-0.251	-0.176	-0.099	-0.024					
-30	-0.274	-0.199	-0.121	-0.041	0.032	0.107				-0.274	-0.197	-0.12	-0.045	0.025	0.1			
0		-0.229	-0.149	-0.077	0.002	0.077	0.156	0.23			-0.229	-0.15	-0.076	-0.002	0.074	0.155	0.226	
30				-0.093	-0.019	0.05	0.123	0.196	0.274				-0.098	-0.026	0.048	0.123	0.196	0.27
50						0.023	0.105	0.178	0.247						0.027	0.101	0.172	0.244

This experimental technique has two other uses. First, it shows the number of entries after making cuts, and therefore, which cuts should not be used because they leave too few entries. And secondly, they give us a root-mean-square (rms) value, or standard deviation of our results. Table 5 displays the average experimental rms values for each absorber run.

The theoretical results are obtained using D. Williams theoretical calculations in reference [4]. The calculations are written in C code, and J. Feldt edited this code so one could input the parameters and obtain the theoretical results easily. The code can be found on the web at: <http://scipp.ucsc.edu/~nate/macros>, and the theoretical roving displacements for different roving module depths are in tables 16, 17, and 18 in appendix B, with the standard deviations in table 5 below. As expected, these uncertainties depend only on the depth inside of the PMMA.

Table 5: Root-mean-squares of the roving displacement distributions, and theoretical sigmas from the theoretical calculation.

run:	average experimental RMS (cm)	theoretical sigma (cm)	average all angle RMS (cm)
405	0.034	0.025	0.037
252	0.041	0.033	0.047
329	0.040	0.028	0.044

The experimental RMS, however, depends on the bin width of the angular and positional experimental data. And, also, the dispersion of the beam, which contributes to the fact that the experimental RMS increases with the depth of the beam.

Comparing the correlation-based results, we subtract the entries in tables 12, 3, and 13, from the entries in tables 2, 10, and 11, respectively, to get tables 6 (below), 19, and 20 (appendix B). The differences are small, confirming that both correlation-based results are valid.

Table 6: Differences between roving displacements obtained using the two correlation methods: materialExit and exitAng correlations for run 405. The plane 1 (horizontal) differences are on the right side.

ang	-0.4	-0.3	-0.2	-0.1	0	0.1	0.2	0.3	0.4	-0.4	-0.3	-0.2	-0.1	0	0.1	0.2	0.3	0.4
-50	-0.004	-0.001	-0.005	-0.005						-0.001	-0.001	0.003	0.003					
-30	0.004	0.003	-0.001	-0.003	-0.007	-0.006				0.000	-0.001	-0.001	-0.002	-0.004	-0.006			
0		0.008	0.003	0.001	-0.001	-0.001	-0.002	-0.011	0.000		0.003	0.000	0.000	-0.001	0.000	0.001	0.000	
30				0.004	0.005	0.005	0.002	-0.001	-0.001				-0.002	-0.001	0.001	0.001	0.000	-0.001
50						0.015	0.009	0.008	0.003						0.006	0.004	0.001	-0.003

Next, we do a similar comparison of the results we obtained from the one-dimensional roving displacement histograms. The next table (table 7) and tables 21, and 22 (in appendix B), show the differences between entries in tables 14, 15 and 4, and 2, 10, and 11, respectively. These differences are also small, exhibiting the fact that using the means of the roving displacement distributions as our results is acceptable.

Table 7: Differences between roving displacements obtained using the materialExit correlations and the one-dimensional histograms for run 329. The plane 1 (horizontal) differences are on the right side.

ang	-0.4	-0.3	-0.2	-0.1	0	0.1	0.2	0.3	0.4	-0.4	-0.3	-0.2	-0.1	0	0.1	0.2	0.3	0.4
-50	-0.007	0.000	-0.007	0.005	0.000	0.002				0.002	0.000	-0.004	-0.005	0.002	0.004			
-30	-0.002	0.001	-0.001	-0.004	0.000	0.000	-0.004	-0.002		-0.001	-0.001	-0.004	-0.002	0.002	0.002	-0.003	0.002	
0		0.002	-0.002	0.002	-0.001	0.000	-0.004	-0.002			0.001	-0.002	0.000	0.002	0.002	0.000	0.002	
30				-0.003	-0.004	0.001	0.002	0.003	0.000				-0.004	-0.001	-0.001	-0.001	0.001	0.001
50						0.005	-0.002	-0.001	0.005					0.000	0.001	0.006	0.009	0.009

Now that we have confirmed the fact that all the results agree with each other, we can compare them to the theoretical predictions of reference [4]. By subtracting tables 17, 16, and 18 from tables 10, 2, and 11, we produce the comparison tables 8 (below), 23, and 24 (in appendix B) respectively.

Table 8: Run 252, difference between experimental and theoretical roving displacements. The plane 1 (horizontal) differences are on the right side.

ang	-0.4	-0.3	-0.2	-0.1	0	0.1	0.2	0.3	0.4	-0.4	-0.3	-0.2	-0.1	0	0.1	0.2	0.3	0.4
-50	-0.017	-0.017	-0.018	-0.019	0.000	-0.011				-0.019	-0.018	-0.019	-0.019	-0.009	-0.008			
-30	-0.011	-0.010	-0.011	-0.010	-0.010	-0.011				-0.013	-0.012	-0.011	-0.009	-0.009	-0.008			
0		-0.002	-0.002	0.000	0.000	0.001	0.002	0.002			-0.005	-0.003	-0.001	0.001	0.002	0.005	0.006	
30				0.013	0.013	0.012	0.013	0.013	0.013				0.006	0.008	0.010	0.013	0.015	0.018
50						0.018	0.017	0.016	0.016						0.013	0.013	0.013	0.014

One aspect of the data analysis that worried us was whether we should have only used data from the center of the detectors, to avoid analyzing bad data. We showed that this did not affect our results by cutting events that had hits on the first module before strip 70 and after strip 121, and observing that one of the more sensitive correlations did not change (see figures 19 and 20).

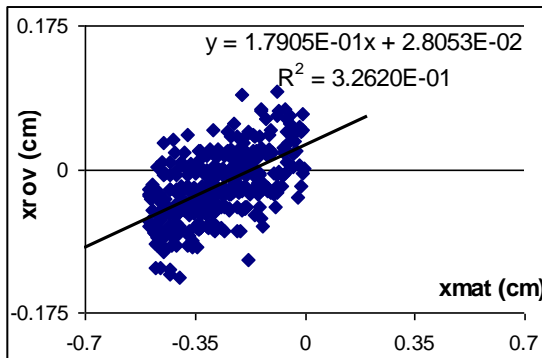


Figure 19: Correlation between xrov and xmat for run 405 exitAng = -50 +- 5mrad, $-0.5 < xmat < 0$ cm, and only strips 70 through 121 are hit on the first plane 0 detector.

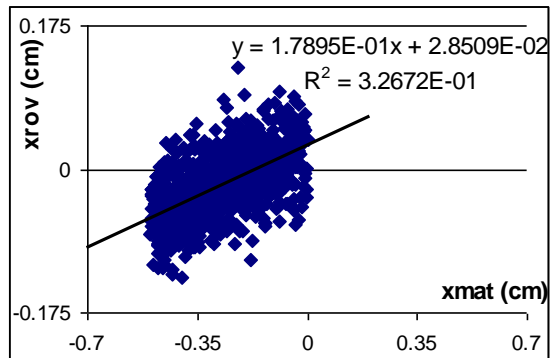


Figure 20: Same as figure 19 except using all hits on first module (not cutting strips below 70 and above 121). The linear fit does not change more than 5um with respect to figure 19.

The first proton trajectory plot is done for different material exits over all legitimate exit angles (see figure 21 and table 9). The only cuts are on protons that have exit angles outside of $\pm 80\text{mrad}$ (see figure 11). The agreement between experiment and theory is very good, but fortuitous as the previous data at different angles has shown.

Table 9: Experimental and theoretical roving displacements used to produce figure 21. $-80\text{mrad} < \text{exitAng} < 80\text{mrad}$.

Run	matEntrance	matExit	Xmat	zrov(cm)	experimental:		theoretical:	
					xrov	sigma	xrov	sigma
405	0	18.01	-0.4	5.134	-0.058	0.038	-0.050	0.025
329	0	18.01	-0.4	13.884	-0.264	0.043	-0.258	0.028
252	0	18.01	-0.4	7.634	-0.112	0.051	-0.101	0.033
405	0	18.01	-0.2	5.134	-0.028	0.037	-0.024	0.025
329	0	18.01	-0.2	13.884	-0.133	0.046	-0.128	0.028
252	0	18.01	-0.2	7.634	-0.058	0.047	-0.050	0.033
405	0	18.01	0.1	5.134	0.016	0.037	0.013	0.025
329	0	18.01	0.1	13.884	0.069	0.046	0.064	0.028
252	0	18.01	0.1	7.634	0.028	0.046	0.025	0.033
405	0	18.01	0.3	5.134	0.043	0.036	0.037	0.025
329	0	18.01	0.3	13.884	0.201	0.045	0.192	0.028
252	0	18.01	0.3	7.634	0.085	0.047	0.074	0.033

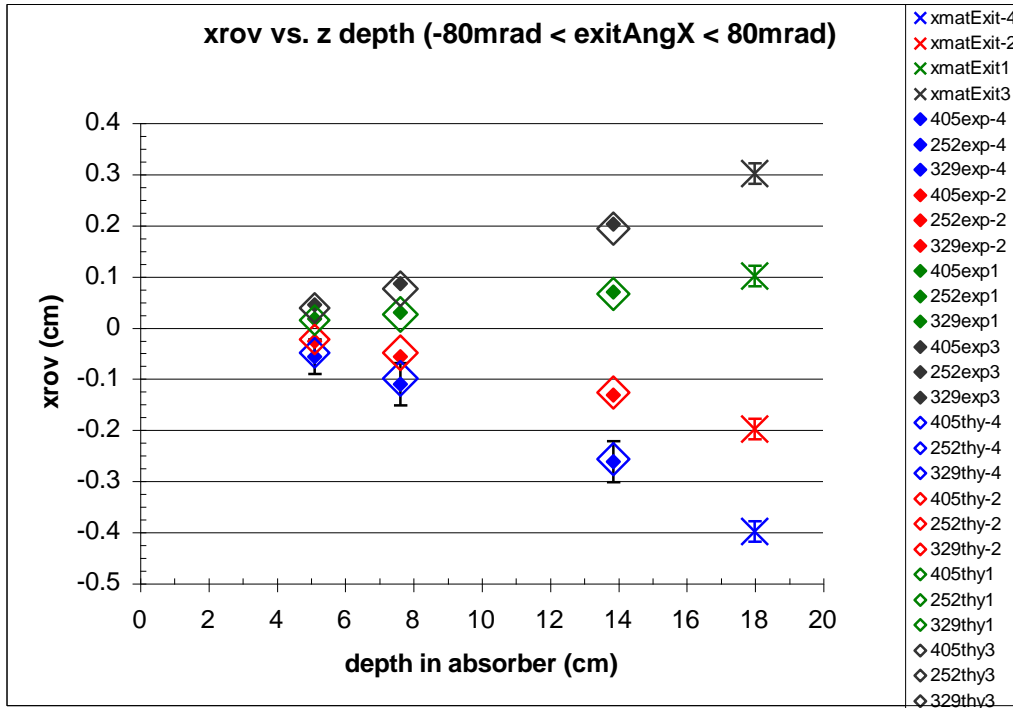


Figure 21: Plot of experimental and theoretical roving displacements for protons with $xmat (\pm 0.02\text{cm}) = -0.4, -0.2, 0.1, \text{ and } 0.3$ cm, and any exitAngX between -80mrad and 80mrad . The theoretical predictions are open rhombus shaped and are approximately the size of their uncertainty. The error bars on the experimental results for $\text{materialExitx} = -0.4$ show their uncertainty, this is the average uncertainty and applies to the corresponding roving displacements in each run for different materialExits .

For all runs, the experimentally found roving displacement of protons that leave the absorber at zero angle, is never more than 80 microns from the theoretical prediction of the roving displacement. This agreement is shown graphically in figure 22.

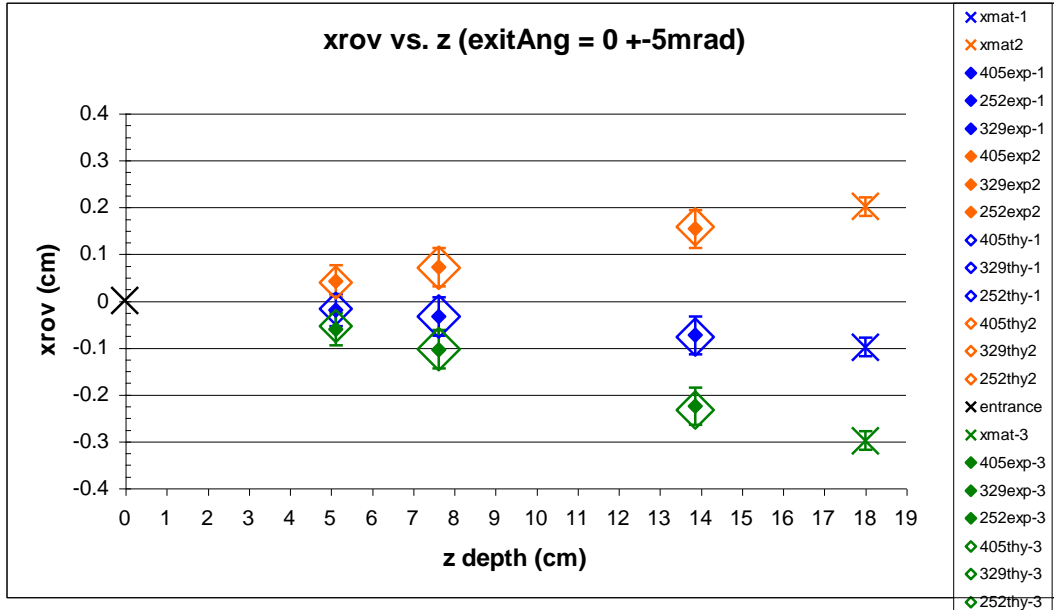


Figure 22: A plot of experimental and theoretical roving displacement for protons with $\text{exitAng} = 0 \pm 5\text{mrad}$, and $\text{materialExit} (\pm 0.02\text{cm}) = -0.3, -0.1, \text{ or } 0.2\text{cm}$. The theoretical predictions are open rhombus shaped and are the size of their uncertainty. The error bars on the experimental results show their RMS.

As we move to other angles, the agreement is worse. If the exitAng and materialExit displacement have opposite signs we observe discrepancies between experiment and theory. This is shown for $\text{exitAng} = 30\text{mrad}$, $\text{materialExit} = -0.1\text{cm}$ in figure 23 (the blue proton trajectory):

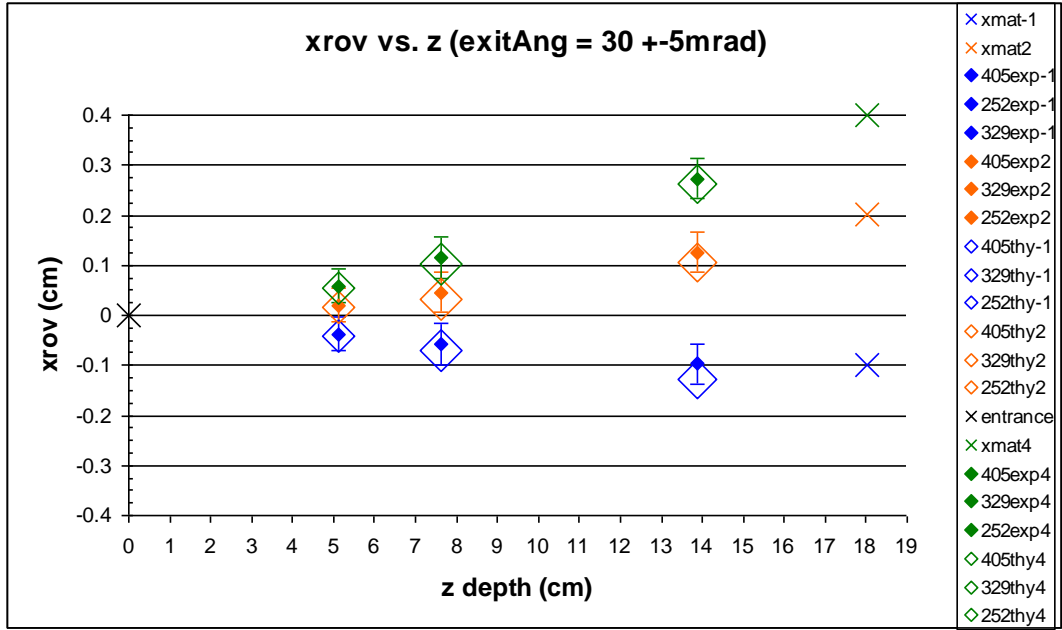


Figure 23: A plot of experimental and theoretical roving displacement for protons with $\text{exitAng} = 30 \pm 5 \text{ mrad}$, and $\text{materialExit} (\pm 0.02 \text{ cm}) = -0.1, 0.2, \text{ or } 0.4 \text{ cm}$. The theoretical predictions are open rhombus shaped and are the size of their uncertainty. The error bars on the experimental results show their uncertainty. This plot shows how the experimentally determined roving displacement of a proton with a positive angle and negative material exit has less agreement with the theoretical prediction.

At even greater angles, such as $\text{exitAng} = -50 \pm 5 \text{ mrad}$, there appears to be a systematic offset between the theoretically predicted and the experimentally determined roving displacement. This is shown in figure 24 (take note that this figure is on a different scale than the previous figures).

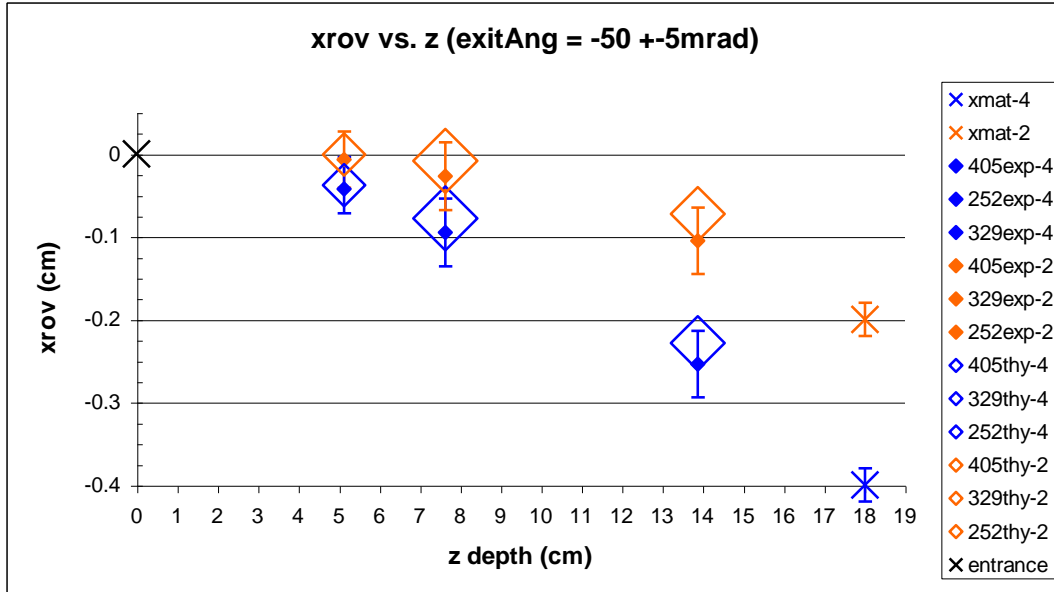


Figure 24: A plot of experimental and theoretical roving displacements for protons with exitAngX = -50 +- 5mrad, and materialExitx (+- 0.02cm) = -0.2, or -0.4cm. The theoretical predictions are open rhombus shaped and are the size of their uncertainty. The error bars on the experimental results show their uncertainty. This plot shows that at large exit angles there is some systematic offset between the theory and experiment.

Figure 25 shows different experimental and theoretical trajectories of protons that have the same material exit displacement, but a variety of exit angles. Though the theory and experiment follow each other somewhat, there is a systematic offset as the proton travels farther into the absorber. In all cases the systematic offsets are less than 200um. Adding this uncertainty to observed RMS of 340, 410, and 400um results in an accuracy of better than 600um, without a systematic correction.

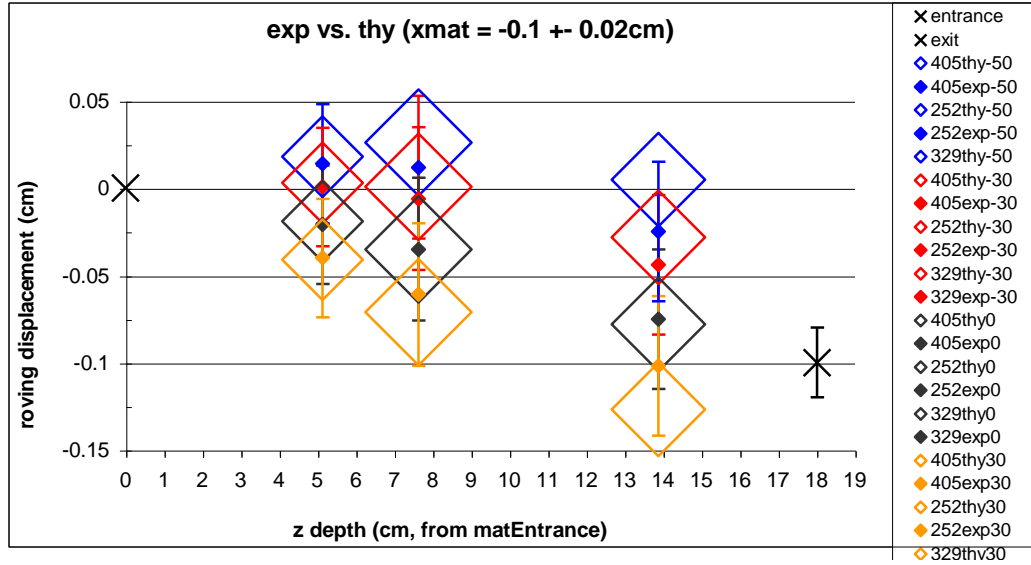


Figure 25: A plot of experimental and theoretical roving displacements for protons with $x_{mat} = -0.1 \pm 0.02$ cm, and $exitAngX$ (± 5 mrad) = -50, -30, 0, or 30 mrad. The theoretical predictions are open rhombus shaped and are approximately the size of their uncertainty. The error bars on the experimental results show their uncertainty. This plot shows that at large exit angles there is some systematic offset between the theory and experiment of the order 200 μ m.

Conclusion

We find good agreement between experiment and theory for small angles (0, ± 30 mrad). The agreement at larger angles is also relatively good. The position of the proton inside the PMMA can be determined to about 400 μ m with corrections for systematic errors, or to 600 μ m without corrections.

The fact that a proton that leaves the phantom with a larger angle will deviate further from the theoretical prediction of the MLP of a charged particle than a proton with a smaller angle suggests that either something is wrong with our analysis or the calculation of the MLP. At first one might guess that the misalignment that was still evident after the dispersion correction (figure 10) could be responsible for the +200 μ m disagreement. This could not be since the offset we observe is in both directions (see figure 25).

This leads me to conclude that the MLP calculation described in reference [4] does not hold with precise accuracy for protons traversing PMMA that are scattered at great angles. This could be due to either of two reasons. The first being the fact that the MLP calculation is based on the approximation that MS follows a gaussian distribution [3]. This approximation may hold for the majority of the particles that have small displacements and angles, but the less frequent protons, that would appear in the tail of the distribution, may not follow the gaussian tail. The final reason that the MS technique of calculating the MLP of our protons could be wrong is that there are other effects besides MS that may need to be accounted for, such as nuclear interactions, and resolution effects due to finite binning. Dr. Pablo Cirrone, another of our Italian collaborators, is currently working on a Monte Carlo simulation of our experiment that will take other effects into account [8]. We expect excellent agreement between this simulation and our experimental results.

As for the future of the pCT project, another beam run at LLUMC has already been performed. Currently the data from this 2006 run is being analyzed at SCIPP by Professor Hartmut Sadrozinski, and students Maureen Petterson and Dominic Lucia. Their goal is to detect small changes in density by closely analyzing the energy of each proton. With the positions better than 600um, as shown above, and energy known for every proton, image reconstruction is the next step toward making pCT a reality, and may not be far away.

Appendix A: Figures

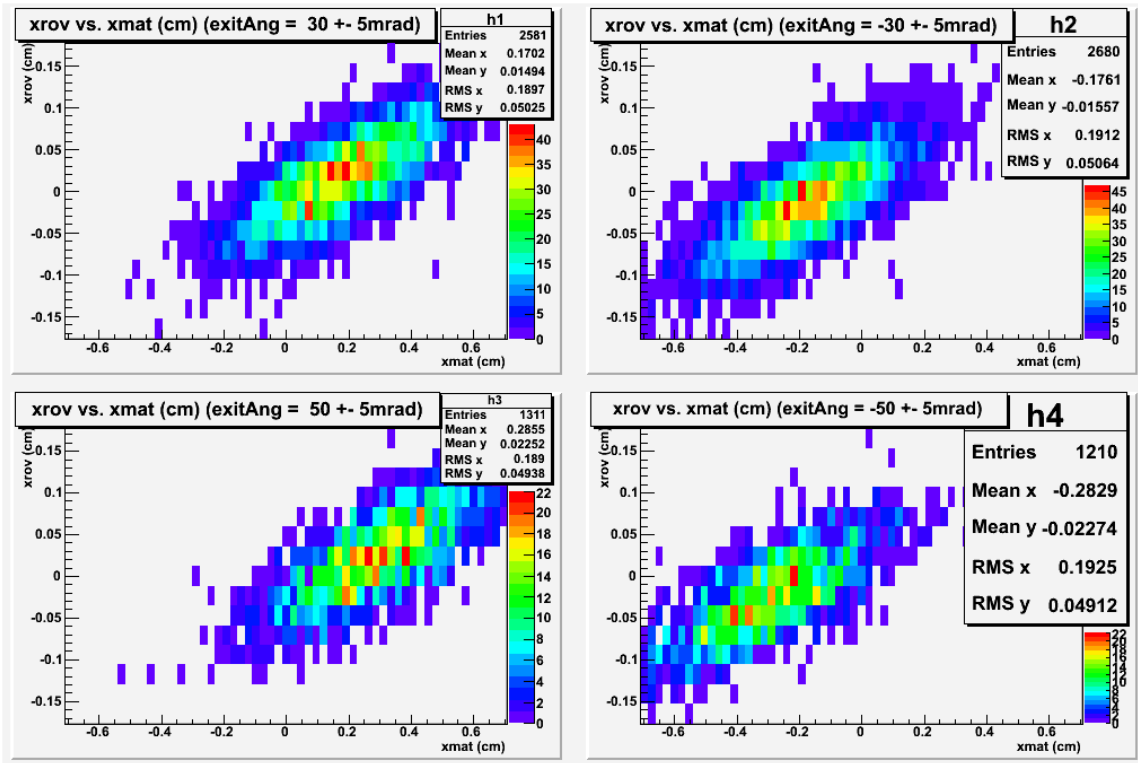


Figure A1: ROOT plots of x_{rov} vs. x_{mat} for different exitAng (see titles of plots for which exitAng). Run 405.

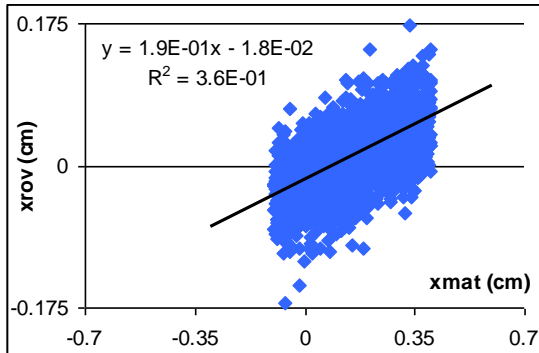


Figure A2: Run 405 excel plot of x_{rov} vs. x_{mat} for exitAng = 30 ± 5 mrad and $-0.1 \text{ cm} < x_{mat} < 0.4 \text{ cm}$.

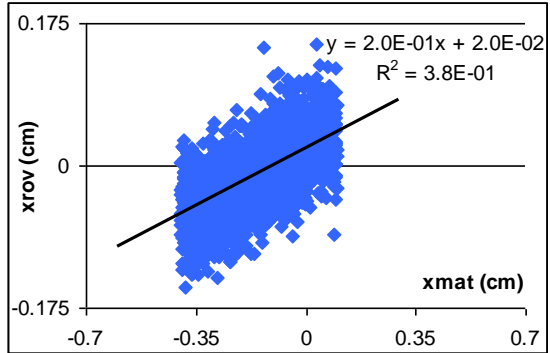


Figure A3: Run 405 excel plot of x_{rov} vs. x_{mat} for exitAng = -30 ± 5 mrad and $-0.4 \text{ cm} < x_{mat} < 0.1 \text{ cm}$.

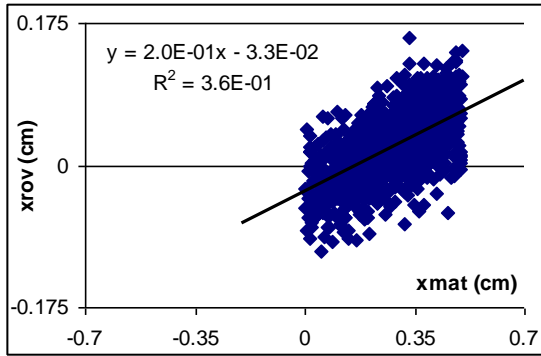


Figure A4: Run 405 excel plot of xrov vs. xmat for exitAng = 50 +/- 5mrad and 0cm < xmat < 0.5cm.

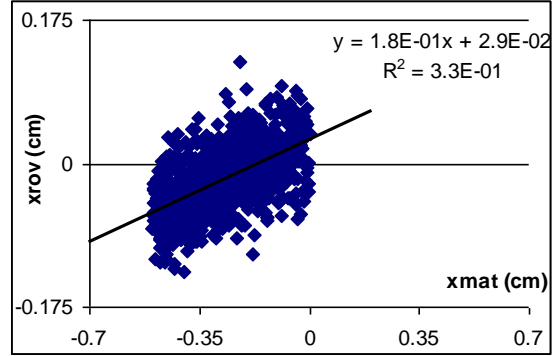


Figure A5: Run 405 excel plot of xrov vs. xmat for exitAng = -50 +/- 5mrad and -0.5cm < xmat < 0cm.

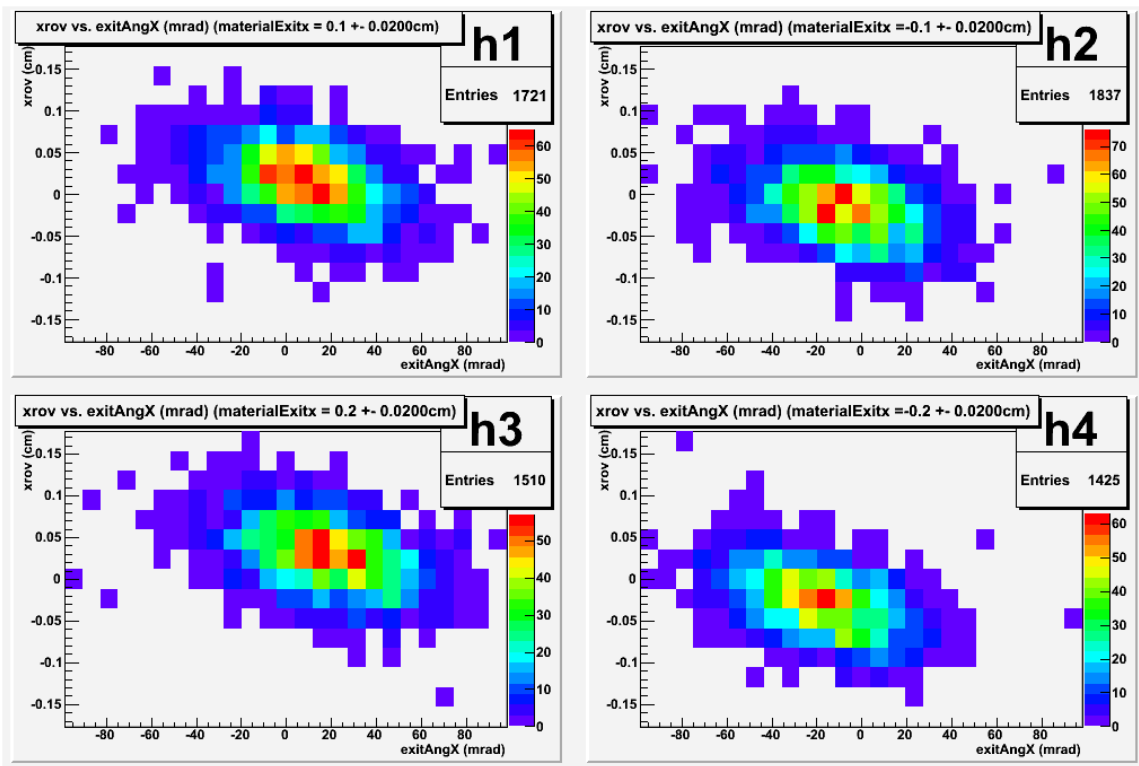


Figure A6: ROOT plots of xrov vs. exitAngX for different materialExitx (see titles of plots for which material exit displacements). Run 405.

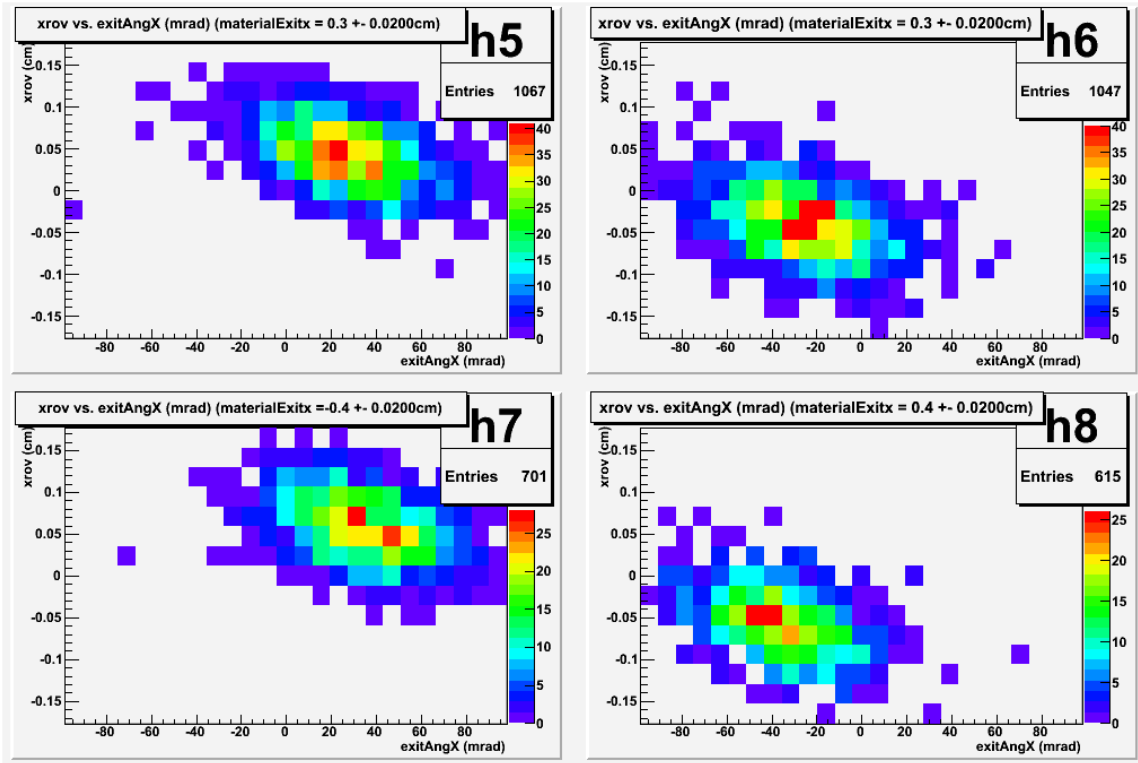


Figure A7: ROOT plots of xrov vs. exitAngX for different materialExitx (see titles of plots for which material exit displacements). Run 405.

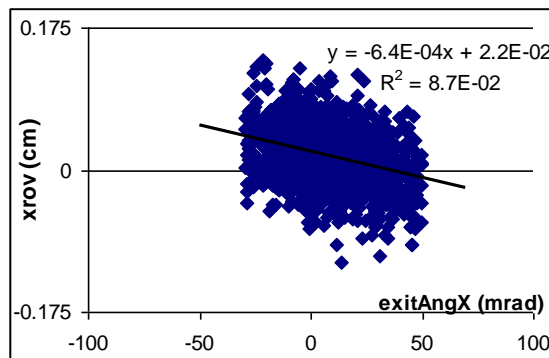


Figure A8: Run 405 excel plot of xrov vs. exitAngX for $xmat = 0.10 \pm 0.02\text{cm}$ and $-30\text{mrad} < \text{exitAngX} < 50\text{mrad}$.

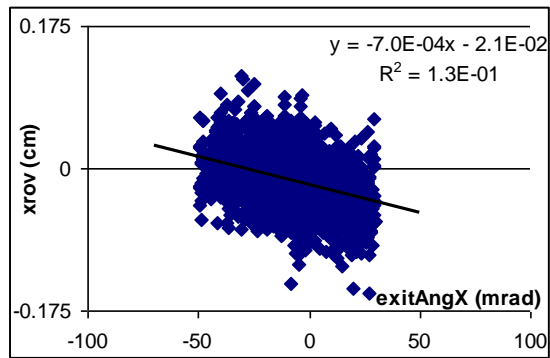


Figure A9: Run 405 excel plot of xrov vs. exitAngX for $xmat = -0.10 \pm 0.02\text{cm}$ and $-50\text{mrad} < \text{exitAngX} < 30\text{mrad}$.

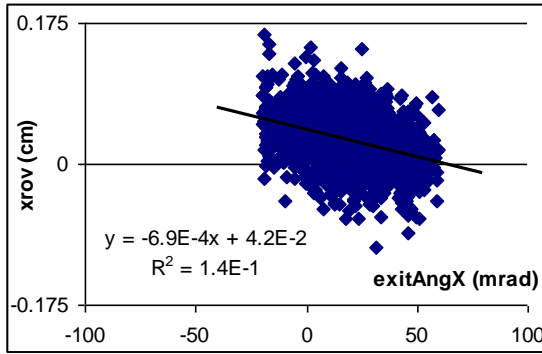


Figure A10: Run 405 excel plot of xrov vs. exitAngX for $x_{mat} = 0.20 \pm 0.02\text{cm}$ and $-20\text{mrad} < \text{exitAngX} < 60\text{mrad}$.

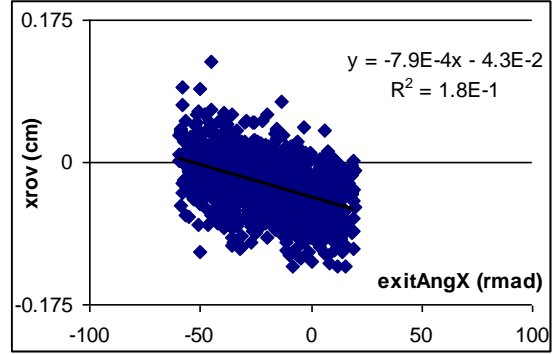


Figure A11: Run 405 excel plot of xrov vs. exitAngX for $x_{mat} = 0.20 \pm 0.02\text{cm}$ and $-60\text{mrad} < \text{exitAngX} < 20\text{mrad}$.

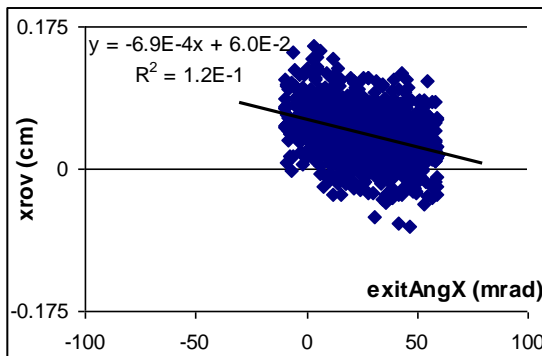


Figure A12: Run 405 excel plot of xrov vs. exitAngX for $x_{mat} = 0.30 \pm 0.02\text{cm}$ and $-10\text{mrad} < \text{exitAngX} < 60\text{mrad}$.

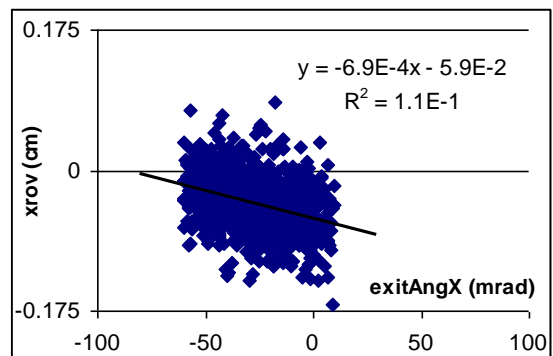


Figure A13: Run 405 excel plot of xrov vs. exitAngX for $x_{mat} = -0.30 \pm 0.02\text{cm}$ and $-60\text{mrad} < \text{exitAngX} < 10\text{mrad}$.

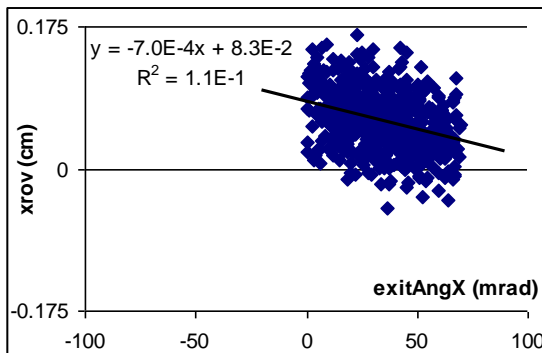


Figure A14: Run 405 excel plot of xrov vs. exitAngX for $x_{mat} = 0.40 \pm 0.02\text{cm}$ and $0\text{mrad} < \text{exitAngX} < 70\text{mrad}$.

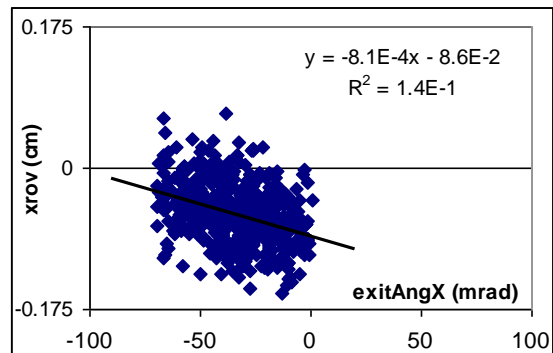


Figure A15: Run 405 excel plot of xrov vs. exitAngX for $x_{mat} = -0.40 \pm 0.02\text{cm}$ and $-70\text{mrad} < \text{exitAngX} < 0\text{mrad}$.

The rest of the roving displacement correlation graphs for plane 1 and both planes for runs 252 and 329 were left out of the appendix because they are similar and there are too many of them. They can be found on the web at (replace 252 with 405 or 329) http://scipp.ucsc.edu/~nate/252/xyrov_vs_xymat/, and http://scipp.ucsc.edu/~nate/252/xyrov_vs_exitAng/.

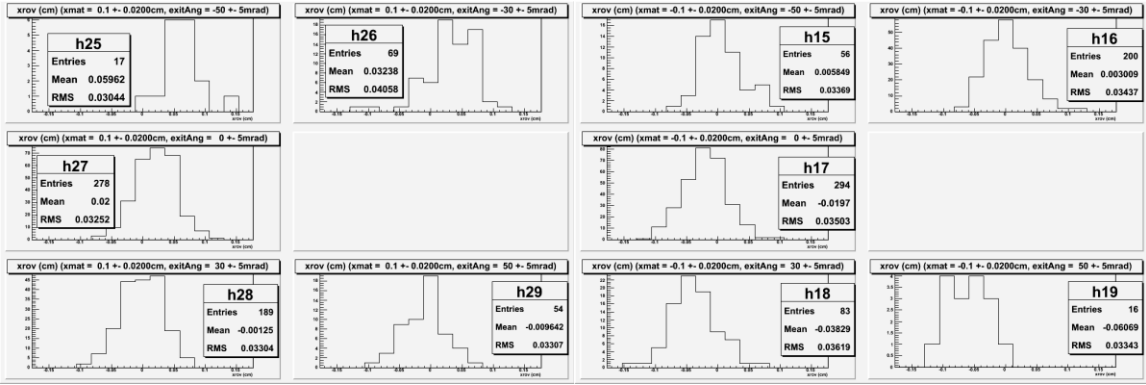


Figure A16: Run 405 plane 0 roving displacements for $xmat = 0.10 \pm 0.020cm$ and each exit angle.

Figure A17: Run 405 plane 0 roving displacements for $xmat = -0.10 \pm 0.020cm$ and each exit angle.

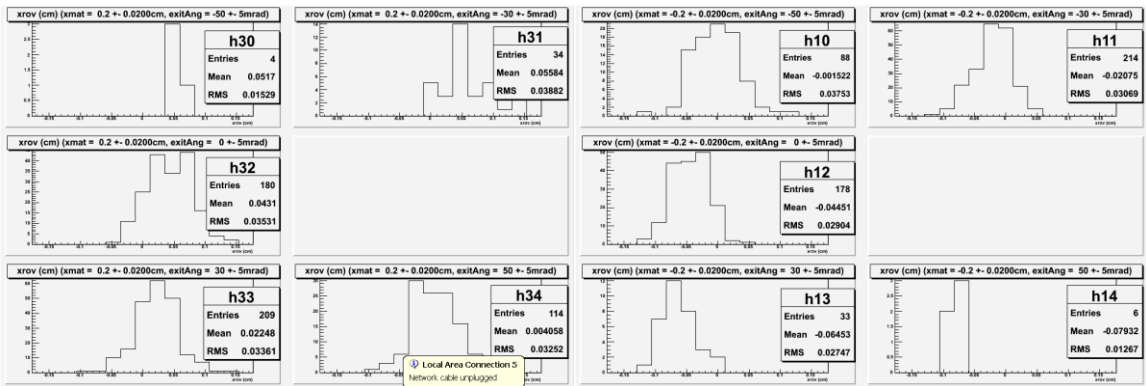


Figure A18: Run 405 plane 0 roving displacements for $xmat = 0.20 \pm 0.020cm$ and each exit angle.

Figure A19: Run 405 plane 0 roving displacements for $xmat = -0.20 \pm 0.020cm$ and each exit angle.

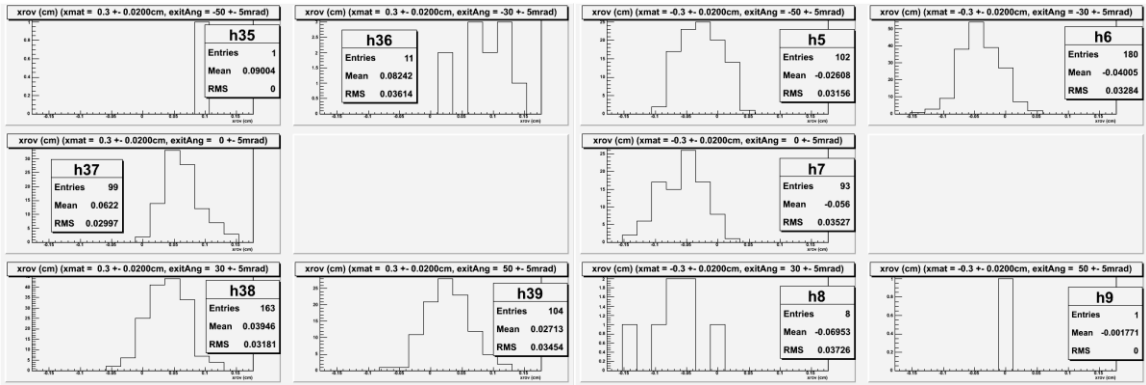


Figure A20: Run 405 plane 0 roving displacements for $xmat = 0.30 \pm 0.020cm$ and each exit angle.

Figure A21: Run 405 plane 0 roving displacements for $xmat = -0.30 \pm 0.020cm$ and each exit angle.

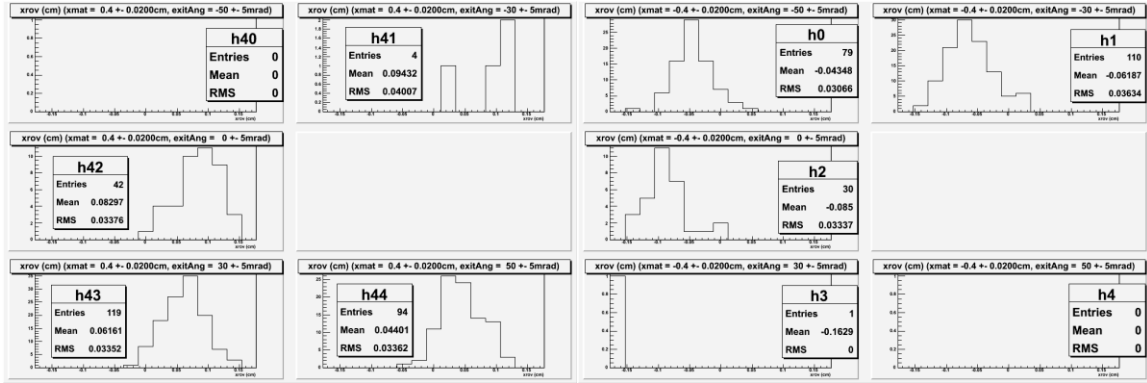


Figure A22: Run 405 plane 0 roving displacements for $xmat = 0.40 \pm 0.02cm$ and each exit angle.

Figure A23: Run 405 plane 0 roving displacements for $xmat = -0.40 \pm 0.02cm$ and each exit angle.

The rest of the one-dimensional roving displacement histograms for plane 1 and both planes for runs 252 and 329 were left out of the appendix because they are similar and there are too many of them. They can be found on the web at (replace 329 with 252 or 405) http://scipp.ucsc.edu/~nate/329/rov_disp_hists.

Appendix B: Tables

Table 10: Roving displacement versus materialExit displacement correlations for different exit angles (+-5mrad) and displacements in materialExit for run 252. The results are the roving displacements in cm.

ang	-0.4	-0.3	-0.2	-0.1	0	0.1	0.2	0.3	0.4	-0.4	-0.3	-0.2	-0.1	0	0.1	0.2	0.3	0.4
-50	-0.095	-0.061	-0.027	0.007						-0.097	-0.062	-0.028	0.007					
-30	-0.113	-0.078	-0.044	-0.009	0.026	0.06				-0.115	-0.08	-0.044	-0.008	0.027	0.063			
0		-0.106	-0.071	-0.035	2E-04	0.036	0.071	0.106			-0.109	-0.072	-0.036	7E-04	0.037	0.074	0.11	
30				-0.058	-0.023	0.011	0.046	0.081	0.115				-0.065	-0.028	0.009	0.046	0.083	0.12
50						-0.008	0.026	0.06	0.094						-0.013	0.022	0.057	0.092

Table 11: Roving displacement versus materialExit displacement correlations for different exit angles (+-5mrad) and displacements in materialExit for run 329. The results are the roving displacements in cm.

ang	-0.4	-0.3	-0.2	-0.1	0	0.1	0.2	0.3	0.4	-0.4	-0.3	-0.2	-0.1	0	0.1	0.2	0.3	0.4
-50	-0.254	-0.179	-0.105	-0.03						-0.249	-0.176	-0.103	-0.029					
-30	-0.276	-0.199	-0.122	-0.045	0.032	0.109				-0.274	-0.199	-0.123	-0.048	0.028	0.103			
0		-0.226	-0.151	-0.075	7E-04	0.076	0.152	0.228			-0.228	-0.152	-0.076	4E-05	0.076	0.152	0.228	
30				-0.097	-0.023	0.051	0.125	0.199	0.273				-0.102	-0.027	0.047	0.122	0.197	0.271
50						0.028	0.102	0.177	0.251						0.027	0.102	0.178	0.253

Table 12: Theoretical and horizontal experimental results obtained using the roving displacement versus exitAng correlations for run 405. The results are the roving displacements in cm.

ang	-0.4	-0.3	-0.2	-0.1	0	0.1	0.2	0.3	0.4	-0.4	-0.3	-0.2	-0.1	0	0.1	0.2	0.3	0.4
-50	-0.045	-0.025	-0.003	0.014						-0.046	-0.025	-0.008	0.014					
-30	-0.061	-0.039	-0.019	2E-04	0.018	0.041				-0.061	-0.04	-0.021	7E-04	0.023	0.045			
0		-0.059	-0.043	-0.021	-8E-04	0.022	0.042	0.06			-0.063	-0.04	-0.019	0.001	0.021	0.04	0.062	
30				-0.042	-0.019	0.002	0.022	0.04	0.062				-0.04	-0.02	0.002	0.018	0.04	0.061
50						-0.011	0.008	0.026	0.048						-0.018	0.003	0.025	0.048

Table 13: Theoretical and horizontal experimental results obtained using the roving displacement versus exitAng correlations for run 329. The results are the roving displacements in cm.

ang	-0.4	-0.3	-0.2	-0.1	0	0.1	0.2	0.3	0.4	-0.4	-0.3	-0.2	-0.1	0	0.1	0.2	0.3	0.4
-50	-0.25	-0.178	-0.1	-0.027						-0.251	-0.176	-0.101	-0.025					
-30	-0.271	-0.198	-0.12	-0.046	0.028	0.103				-0.275	-0.197	-0.121	-0.044	0.026	0.104			
0		-0.229	-0.151	-0.074	0.001	0.076	0.15	0.227			-0.227	-0.15	-0.073	4E-05	0.074	0.15	0.23	
30				-0.102	-0.026	0.049	0.122	0.197	0.272				-0.102	-0.026	0.045	0.124	0.197	0.275
50						0.031	0.104	0.177	0.253						0.026	0.106	0.175	0.251

Table 14: Roving displacement as a function of materialExit (+-0.02cm) and exitAng (+-5mrad) from the one-dimensional roving displacement distribution histograms for run 405.

ang	-0.4	-0.3	-0.2	-0.1	0	0.1	0.2	0.3	0.4	-0.4	-0.3	-0.2	-0.1	0	0.1	0.2	0.3	0.4
-50	-0.043	-0.026	-0.002	0.006						-0.048	-0.027	-0.012	0.017					
-30	-0.062	-0.04	-0.021	0.003	0.019	0.032				-0.062	-0.039	-0.024	-0.001	0.021	0.043			
0		-0.056	-0.045	-0.02	-9E-04	0.02	0.043	0.062			-0.061	-0.039	-0.019	0.003	0.022	0.041	0.059	
30				-0.038	-0.018	-0.001	0.022	0.039	0.062				-0.037	-0.017	0.003	0.022	0.041	0.057
50						-0.01	0.004	0.027	0.044						-0.017	0.008	0.028	0.046

Table 15: Roving displacement as a function of materialExit (+-0.02cm) and exitAng (+-5mrad) from the one-dimensional roving displacement distribution histograms for run 252.

exitAngX	-0.4	-0.3	-0.2	-0.1	0	0.1	0.2	0.3	0.4	-0.4	-0.3	-0.2	-0.1	0	0.1	0.2	0.3	0.4
-50	-0.089	-0.058	-0.033	0.01						-0.095	-0.063	-0.028	0.009					
-30	-0.11	-0.078	-0.043	-0.009	0.027	0.063				-0.111	-0.079	-0.042	-0.005	0.027	0.056			
0		-0.102	-0.074	-0.035	0.004	0.035	0.067	0.108			-0.104	-0.071	-0.03	0.004	0.034	0.074	0.104	
30				-0.06	-0.019	0.009	0.041	0.083	0.113				-0.055	-0.028	0.009	0.041	0.075	0.114
50						-0.017	0.027	0.065	0.091						-0.014	0.027	0.057	0.085

Table 16: Theoretical roving displacements for each parameter combination for run 405.

ang	-0.4	-0.3	-0.2	-0.1	0	0.1	0.2	0.3	0.4
-50	-0.038	-0.019	-0.001	0.018					
-30	-0.053	-0.034	-0.015	0.003	0.022	0.041			
0		-0.056	-0.038	-0.019	0	0.019	0.038	0.056	
30				-0.041	-0.022	-0.003	0.015	0.034	0.053
50						-0.018	0.001	0.019	0.038

Table 17: Theoretical roving displacements for each parameter combination for run 252.

ang	-0.4	-0.3	-0.2	-0.1	0	0.1	0.2	0.3	0.4
-50	-0.078	-0.044	-0.009	0.026					
-30	-0.102	-0.068	-0.033	0.001	0.036	0.071			
0		-0.104	-0.069	-0.035	0	0.035	0.069	0.104	
30				-0.071	-0.036	-0.001	0.033	0.068	0.102
50						-0.026	0.009	0.044	0.078

Table 18: Theoretical roving displacements for each parameter combination for run 329.

ang	-0.4	-0.3	-0.2	-0.1	0	0.1	0.2	0.3	0.4
-50	-0.229	-0.151	-0.073	0.005					
-30	-0.262	-0.184	-0.106	-0.028	0.05	0.127			
0		-0.234	-0.156	-0.078	0	0.078	0.156	0.234	
30				-0.127	-0.05	0.028	0.106	0.184	0.262
50						-0.005	0.073	0.151	0.229

Table 19: Differences between results obtained using the roving displacement versus materialExit correlations and the results obtained using the roving displacement versus exitAng correlations for run 252.

ang	-0.4	-0.3	-0.2	-0.1	0	0.1	0.2	0.3	0.4	-0.4	-0.3	-0.2	-0.1	0	0.1	0.2	0.3	0.4
-50	-0.001	0.000	0.000	0.000						0.000	-0.002	-0.003	-0.005					
-30	0.001	0.001	0.001	0.001	-0.001	0.001				-0.001	0.000	-0.001	-0.003	-0.001	-0.002			
0		0.001	0.001	0.000	-0.002	0.001	0.000	-0.001			0.000	-0.001	-0.002	0.000	0.001	0.003	0.004	
30				0.003	-0.001	0.002	0.002	0.000	-0.001				-0.004	-0.001	0.002	0.001	0.004	0.005
50						0.000	0.000	-0.003	-0.004					-0.001	-0.006	-0.003	-0.002	

Table 20: Differences between results obtained using the roving displacement versus materialExit correlations and the results obtained using the roving displacement versus exitAng correlations for run 329.

ang	-0.4	-0.3	-0.2	-0.1	0	0.1	0.2	0.3	0.4	-0.4	-0.3	-0.2	-0.1	0	0.1	0.2	0.3	0.4
-50	-0.004	-0.001	-0.005	-0.003						0.002	0.000	-0.002	-0.004					
-30	-0.005	0.000	-0.002	0.001	0.004	0.006				0.000	-0.002	-0.003	-0.003	0.002	0.000			
0		0.002	0.000	-0.001	0.000	0.000	0.002	0.001			-0.001	-0.002	-0.003	0.000	0.002	0.002	-0.002	
30				0.005	0.003	0.002	0.003	0.002	0.001					-0.001	0.002	-0.002	0.000	-0.004
50						-0.003	-0.002	0.000	-0.001						0.001	-0.004	0.002	0.002

Table 21: Differences between results obtained using the roving displacement versus materialExit correlations and the results obtained using the one-dimensional roving displacement histograms for run 405.

ang	-0.4	-0.3	-0.2	-0.1	0	0.1	0.2	0.3	0.4	-0.4	-0.3	-0.2	-0.1	0	0.1	0.2	0.3	0.4
-50	0.003	0.001	0.005	-0.007						-0.002	-0.001	-0.007	0.000					
-30	0.000	0.001	0.000	0.003	-0.001	-0.008				0.000	0.002	-0.003	-0.003	0.000	0.004			
0		0.005	-0.004	0.001	-0.001	-0.001	0.002	0.000			-0.001	0.001	0.000	0.002	0.001	0.000	-0.002	
30				0.002	0.002	-0.002	0.001	-0.002	0.000				0.004	0.004	0.001	0.000	0.001	-0.002
50						0.009	0.000	0.001	-0.004						-0.005	0.001	0.002	0.001

Table 22: Differences between results obtained using the roving displacement versus materialExit correlations and the results obtained using the one-dimensional roving displacement histograms for run 252.

ang	-0.4	-0.3	-0.2	-0.1	0	0.1	0.2	0.3	0.4	-0.4	-0.3	-0.2	-0.1	0	0.1	0.2	0.3	0.4
-50	-0.006	-0.003	0.006	-0.003						-0.002	0.000	0.000	-0.002					
-30	-0.002	0.000	0.000	0.000	-0.001	-0.002				-0.004	-0.001	-0.002	-0.003	0.000	0.006			
0		-0.004	0.004	0.000	-0.004	0.001	0.004	-0.002			-0.005	-0.001	-0.006	-0.004	0.003	0.000	0.006	
30				0.003	-0.004	0.002	0.006	-0.002	0.002				-0.010	0.000	0.000	0.005	0.009	0.006
50						0.009	-0.001	-0.005	0.003						0.001	-0.005	0.001	0.007

Table 23: Run 405, differences between experimental and theoretical results, x and y.

ang	-0.4	-0.3	-0.2	-0.1	0	0.1	0.2	0.3	0.4	-0.4	-0.3	-0.2	-0.1	0	0.1	0.2	0.3	0.4
-50	-0.009	-0.008	-0.006	-0.005						-0.009	-0.007	-0.003	-0.001					
-30	-0.009	-0.007	-0.006	-0.003	-0.002	0.000				-0.008	-0.007	-0.006	-0.004	-0.003	-0.002			
0		-0.005	-0.003	-0.001	0.000	0.002	0.003	0.006			-0.004	-0.002	-0.001	0.001	0.002	0.003	0.006	
30				0.001	0.002	0.004	0.006	0.007	0.009				0.000	0.001	0.002	0.004	0.005	0.007
50						0.000	0.003	0.007	0.010						0.006	0.006	0.007	0.007

Table 24: Run 329, differences between experimental and theoretical results, x and y.

ang	-0.4	-0.3	-0.2	-0.1	0	0.1	0.2	0.3	0.4	-0.4	-0.3	-0.2	-0.1	0	0.1	0.2	0.3	0.4
-50	-0.025	-0.028	-0.032	-0.035						-0.020	-0.025	-0.030	-0.034					
-30	-0.014	-0.015	-0.016	-0.017	-0.018	-0.018				-0.012	-0.015	-0.017	-0.020	-0.022	-0.024			
0		0.008	0.005	0.003	0.001	-0.002	-0.004	-0.006			0.006	0.004	0.002	0.000	-0.002	-0.004	-0.006	
30				0.030	0.027	0.023	0.019	0.015	0.011				0.025	0.023	0.019	0.016	0.013	0.009
50						0.033	0.029	0.026	0.022					0.032	0.029	0.027	0.024	

References

- [1] Loma Linda University Medical Center.
<http://www.llu.edu/proton/patient/glossary.html>
- [2] B. Schaffner and E. Pedroni, “The precision of proton range calculations in proton radiotherapy treatment planning: experimental verification of the relation between CT-HU and proton stopping power”, *Phys Med Biol.* 43(6):1579-1592, 1998.
- [3] Particle Data Group, S. Eidelman et al., “Review of Particle Physics”, *Physics Letters B* 592, 1 (2004).
- [4] Williams D. C., “The most likely path of an energetic charged particle through a uniform medium,” *Physics in Medicine and Biology*, vol. 49, pp. 2899–2911, 2004
- [5] R. W. Schulte, V. Bashkirov, T. Li, Z. Liang, K. Mueller, J. Heimann, L. R. Johnson, B. Keeney, H. F.-W. Sadrozinski, A. Seiden, D. C. Williams, L. Zhang, Z. Li, S. Peggs, T. Saratoga, C. Woody, “Conceptual design of a proton computed tomography system for applications in proton radiation therapy”, *IEEE Trans. Nucl. Sci.*, vol 51, no.3, pp 866 – 875, June 2004.
- [6] Heimann J R, “Developing an FPGA-Based Readout for the pCT Detector System,” University of California, Santa Cruz. 2005.
- [7] Feldt J., “Preliminary Tracking Studies for Proton Computed Tomography,” University of California, Santa Cruz. 2005.
- [8] G. A. P. Cirrone et al, “Detailed Monte Carlo Investigation of a Proton Computed Tomography System”, Poster J03-25, 2005 IEEE NSS-MIC Symposium in Puerto Rico, Oct 2005.